Estimating physical properties of 3U CubeSat's rotation based on photometric observations and solar illumination modeling

Takuro Tsuchikawa, Takao Endo, and Hidenobu Tsuji
Mitsubishi Electric Corporation, Information Technology R&D Center

ABSTRACT

CubeSats have been launched frequently to the low earth orbit (LEO) as important social infrastructure nowadays, while the growing number of CubeSats increases the risks of collisions between on-orbit objects. Therefore, it is important to monitoring the characteristics of CubeSats to reduce such risks. Mitsubishi Electric has been developing optical observation technology for space situational awareness (SSA) using a small optical telescope facility, Ofuna Space Monitoring and Communications center (OSMC), on its premises. In this paper, we aim to confirm the effectiveness of optical observation in understanding the characteristics of CubeSats by performing two tracking observations of a 3U CubeSat and analyses of the light curves thus obtained. We successfully detect the signals from the 3U CubeSat throughout the observations. The light curve obtained in the first observation shows sharp peaks likely due to specular reflection. In the light curve obtained in the second observation, we do not detect such sharp peaks, while a brightness oscillation, probably due to rotation, is detected because of the faster data acquisition than the first. To estimate the angular velocity of rotation, a Fourier analysis and an epoch folding analysis are conducted on the light curve obtained in the second observation. As a result, the rotational angular velocity is successfully estimated to be 1074.6±1.0 deg/s with high accuracy in contrast with 1074 deg/s estimated from the telemetry data. Furthermore, by comparing the one-period light curve profile estimated by epoch folding analysis with a simple illumination model, we find that the 3U CubeSat is likely to rotate around the short axis.

1. INTRODUCTION

Satellites have become important social infrastructure in recent years. A lot of CubeSats, which is about several tens of centimeters in size and weigh several kilograms, have been launched frequently to the low earth orbit (LEO), while such the growing number of satellites increases the risks of collisions between on-orbit objects. To reduce such risks, space situational awareness (SSA) has been attracting attention for the purpose of monitoring the physical status, such as orbits and attitudes, of satellites and space debris.

Ground-based observations using small-aperture optical telescopes are effective methods for monitoring the status of on-orbit objects, with low installation cost compared to those with radar. Therefore, we have been developing optical observation technology using small-aperture optical telescopes in our institute mainly by observing the light curves of satellites to understand their characteristics. The observed light curves are compared with illumination models considering the optical characteristics of the surfaces of satellite's components to determine the satellite's attitude [1, 2, 3]. In the previous studies, relatively large-sized satellites, which are expected to be bright, are mainly observed, while CubeSats are not observed because it might be difficult to detect them due to their small size. Hence, to verify the observability of small satellites, a 3U CubeSat is selected as the target for the optical tracking observation in this study, the weight and size of which are about 3 kg and 10 cm x 10 cm x 34 cm, respectively. The telemetry data of the 3U CubeSat, which is available to us, indicates a rotation motion. Thus, we also aim to investigate the capability of optical tracking observations to understand the physical states of CubeSats, especially the rotation motion.

2. OBSERVATIONS

2.1 SITE

The observations in this study are conducted in Ofuna Space Monitoring and Communications center (OSMC), constructed in our institute in January 2022 to understand the operational status of spacecraft using ground-based optical observations and advanced data processing of the optical signals obtained. OSMC is located in Kamakura, Japan, whose latitude, longitude and elevation are 35d20m54s N, 139d32m16s E, 15 m, respectively. Fig. 1 shows the appearance of OSMC. The building shown in Fig. 1 is a sliding roof facility, which enables us to efficiently conduct optical observations from the ground.

Fig. 1. Ofuna Space Monitoring and Communications center (OSMC)

2.2 INSTRUMENTATION

As shown in Fig. 2, the instrumental configuration for the satellite observation consists of commercial off-the-shelf (COTS) equatorial mount, telescope, and detector which are summarized in Table 1. The telescope is a Dole-Kirkham type with the aperture size of 36 cm and the focal length of 1623 cm with a focal reducer. The sensor has a high dynamic range of 97.7 dB, allowing us to observe both large and small brightness changes in photometric light curves simultaneously. No optical filter is used to avoid loss of light in terms of signal-to-noise ratio (SNR). The telescope is mounted on an equatorial fork mount. The equatorial fork mount is suitable for high-speed tracking of LEO satellites because the telescope does not be reversed near the zenith. Using the above configuration, we realize a wide field of view (FOV) of 0.8 x 0.8 deg^2, which allows us to initially guide many stars into the FOV and determine the coordinates for each frame. On the other hand, the pixel size is 11 μm corresponding to 1.4 arcsec, which is enough to spatially resolve a typical size of atmospheric seeing, 5 arcsec. Therefore, a single pixel does not collect too much background photons, and thus we can achieve high sensitivity observations.

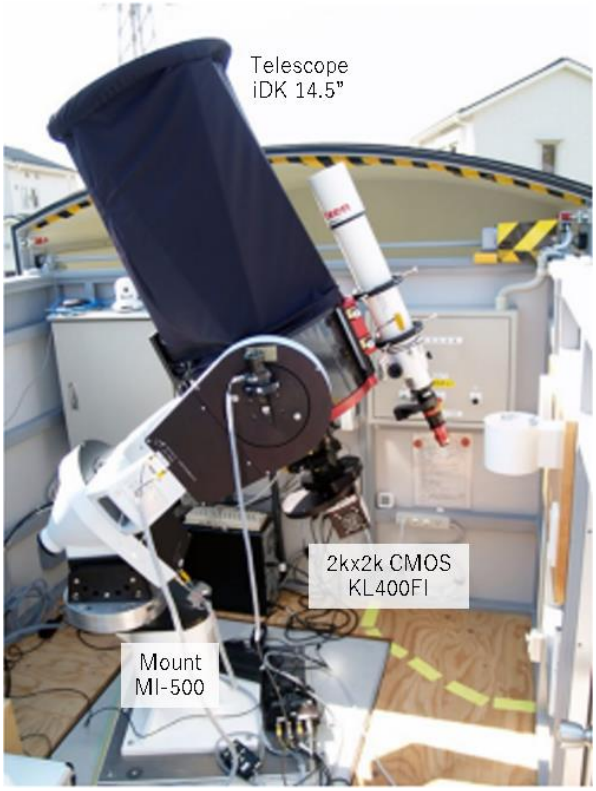

Fig. 2. Configuration of optical telescope for the satellite observation.

Table 1. Summary of instrumental configuration

Component	Specification	
Mount	MI-500 (Mathis Instrument)	Equatorial fork mount
Telescope	iDK 14.5" (AG Optical)	aperture diameter: 37 cm focal length with reducer lens: 1623 mm
Sensor	KL400FI（FLI）	2k x 2k cooled CMOS Pixel size: 11 μm

Parameter	
Frame size	22.528 mm
Pixel FOV	1.4 arcsec
FOV	0.80 deg

2.3 OBSERVATIONS AND RESULTS

Two line elements (TLEs) are widely used to predict the orbits of space objects and are also used in this study. TLEs include orbital information for satellites, rocket bodies, and space debris, monitored and published by North American Aerospace Defense Command (NORAD). Based on the TLEs, the position and velocity vectors of the CubeSat are calculated with the Simplified General Perturbations Satellite Orbit Model 4 (SGP4) orbital propagation code [4, 5]. According to the orbit thus calculated as shown in Fig. 3, we observe the satellite in 2023/3/13 and 2023/4/3 for approximately 5 minutes, and successfully detect the signals throughout the observations, as shown in Fig. 4. The first observation is performed with exposure time of 1 s. Because the detected signal is sufficiently bright in the first observation, the second observation is performed with the exposure time of 0.1 s to improve time resolution.

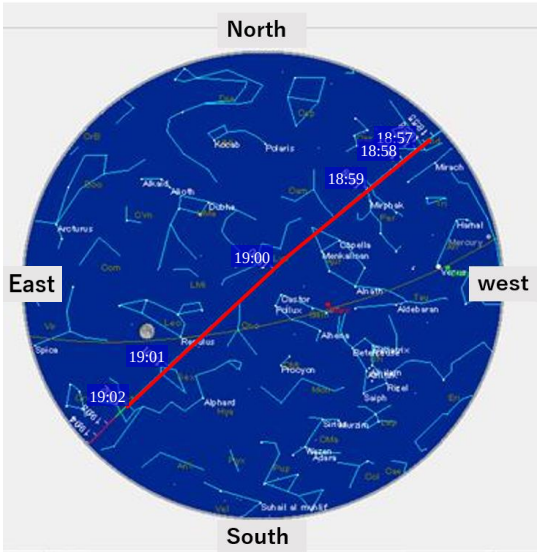

Fig. 3. Satellite orbit tracked in the second observation.

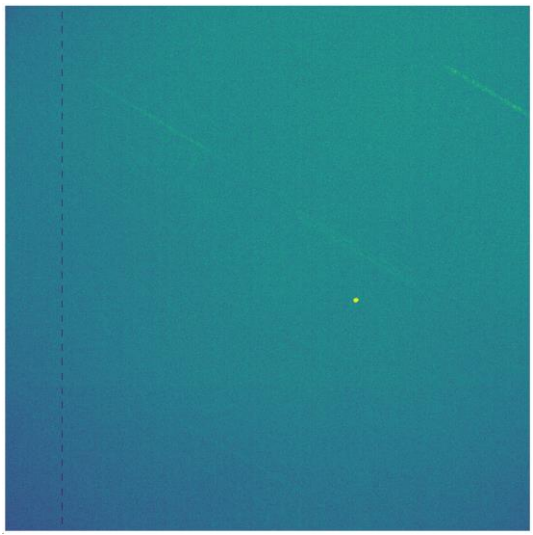
Fig. 4. Detected signal observed on March 13, 2023.

In order to estimate the magnitude of the CubeSat, aperture photometry is performed on each image data after removing the background gradient, where 2.5 times the Kron radius is applied for the aperture radius. Figs. 5 and 6 show the resultant light curves of the 3U CubeSat obtained from the first and second observations, respectively. The light curve in Fig. 5 shows a double peaked profile with the amplitude of about 2 mag and an underlying plateau component with gradual change from 8 to 7 mag. The double peaked profile and the plateau components are likely to originate from the specular and diffuse reflections of sunshine by surfaces of the 3U CubeSat, respectively. In particular, the gradual change of the plateau component is likely to be caused by the changes of the orientation of the CubeSat, the solar phase angle and the distance from the observation site. Compared to the first observation, the light curve in Fig. 6 shows no peaked profile. This is likely because the orientation of the CubeSat and the solar phase angle are different from the first observation. On the other hand, the light curve obtained from the second observation shows brightness oscillations with a short period of less than one second, as shown in the sub figure of Fig. 6, which is expected to originate from the rotational motion of the CubeSat. No brightness oscillation in the first observation is likely attributed to the exposure time longer than the oscillation period. Note that data of the light curve in Fig. 6 is missing around 30 s and 40-60 s due to delays of data transportation.

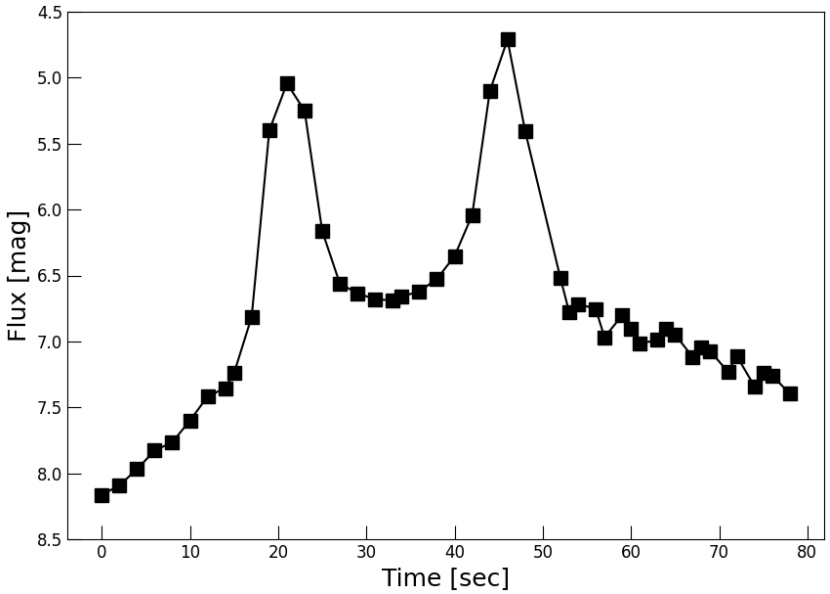

Fig. 5. Light curve of the 3U CubeSat observed with the exposure time of 1 s on March 13, 2023.

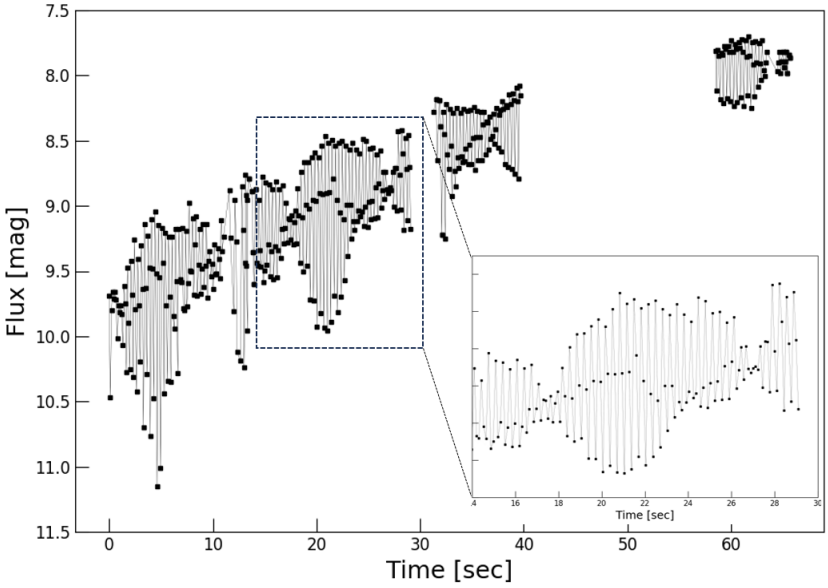

Fig. 6. Light curve of the 3U CubeSat observed with the exposure time of 0.1 s on April 3, 2023.

3. DATA ANALYSIS AND DISCUSSION

3.1 FOURIER ANALYSIS

The brightness oscillation in the light curve shown in Fig. 6 is most likely due to the rotation of the 3U CubeSat. In the past, some studies discussed the angular velocity of the satellite rotation on the basis of such brightness oscillations of light curves [6, 7]. Therefore, we estimate the characteristic frequency of the oscillation by time-frequency analysis to verify the origin of the brightness oscillation. Generally, time-frequency analysis using the Fast Fourier Transform (FFT) requires data sampled at a fixed time interval, but the data in Fig. 6 is not sampled at a fixed time interval as mentioned in section 2.3. On the other hand, the data is sampled at a fixed time interval within the intervals indicated by blue, yellow, green, and red colors in the sub figure in Fig. 7. Therefore, as a simplified method, time-frequency analysis by FFT is performed within the four intervals, and the characteristic frequency of the brightness oscillation is estimated from the spectrum obtained by summing the power spectra in the four intervals shown in Fig. 7. The peak frequencies of the four intervals are found to be around 3 Hz, corresponding to angular velocity of 1100 deg/s. The widths of the spectral peaks differ between the intervals shown in the sub figure, since the maximum time differences are different. Hence, the oscillation frequency can be estimated more accurately using a light curve with larger maximum time difference. Considering the spectral width as the error bar of the peak angular velocity, the angular velocity is 1100 ± 50 deg/s, which is consistent with 1074 deg/s estimated from the telemetry data. Thus, the brightness oscillation on the light curve of the 3U CubeSat is considered to originate from the rotation of the CubeSat itself.

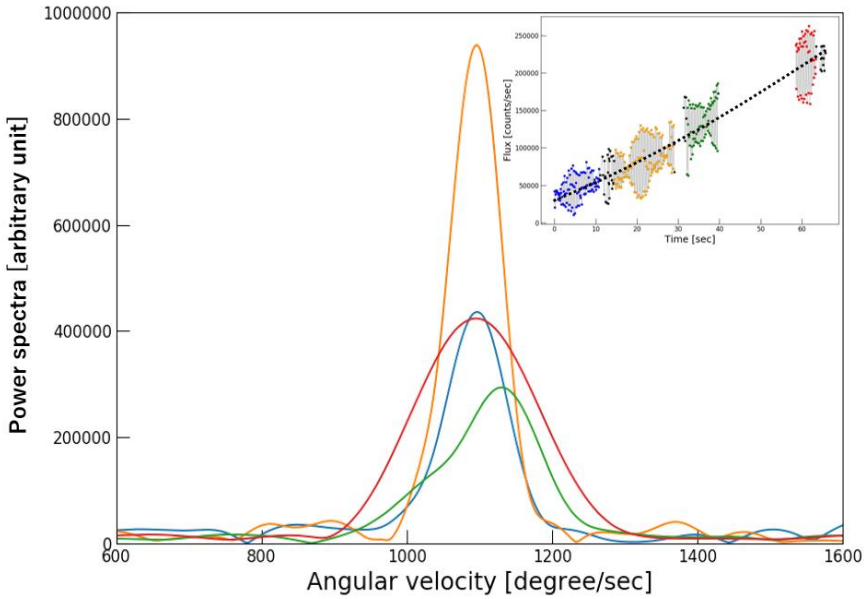

Fig. 7. Power spectra of four intervals in the light curve in Fig. 6. Data in the four intervals is sampled at a fixed time interval. The sub figure shows the light curve shown in Fig. 6. The colors of the spectra correspond to those of the light curves in the sub figure. Only the angular velocity range around the estimate obtained from the telemetry data is shown.

3.2 EPOCH FOLDING ANALYSIS

The angular velocity of the CubeSat is correctly estimated to be 1100 ± 50 deg/s in section 3.1, while the error of 50 deg/s is relatively large compared to the accuracy of the telemetry data. Therefore, we perform the epoch folding analysis, in which the angular velocity can be estimated accurately by assuming that the brightness oscillation is coherent. Furthermore, as opposed to the Fourier analysis, the light curve does not need to be sampled at a fixed time interval in this analysis, which is performed by following steps: first, since the light curve in Fig. 6 rises steadily, we assume an average baseline, as shown by a dotted line in the sub figure of Fig. 7, and subtract it from the original light curve to extract only the component of the brightness oscillation. The baseline is determined by assuming a quadratic function and fitting it to the light curve data. Next, the baseline-subtracted light curve is sectioned at a certain time period, and the data are folded. If the selected time period is not the oscillation period, the folded data is expected to be randomly distributed around 0. On the other hand, If the selected time period is just the oscillation period, the data is expected not to be randomly distributed, and the data points will be distributed on the profile of the one-period light curve. Therefore, to determine whether the folded data is random or aligned on the light curve profile, the folded data is binned. For example, the folded data is divided into 10 bins, and the average flux and average time of the data points in each bin are calculated. If the selected time period is not the oscillation period, the binned data will be close to 0 because of the randomness. On the other hand, if the selected time period is exactly the oscillation period, the binned data is expected to be also aligned on the profile of the one-period light curve. Thus, the angular velocity of the CubeSat can be searched using the amplitude of the binned profile. We utilize the sum of squares of the binned data points as an indicator of the amplitude, and search for the folded period with the largest sum of squares. The resultant angular velocity is 1074.6±1.0 deg/s, which is consistent with the telemetry data with two orders of magnitude better accuracy than the Fourier analysis. Hence, the result further supports the idea that the brightness oscillation originates from the rotation of the 3U CubeSat itself. Fig. 8 shows the folded light curve for two cycles of the brightness oscillation accurately restored in the epoch folding analysis. We can find that the one-period light curve shows two broad peaks with different amplitudes.

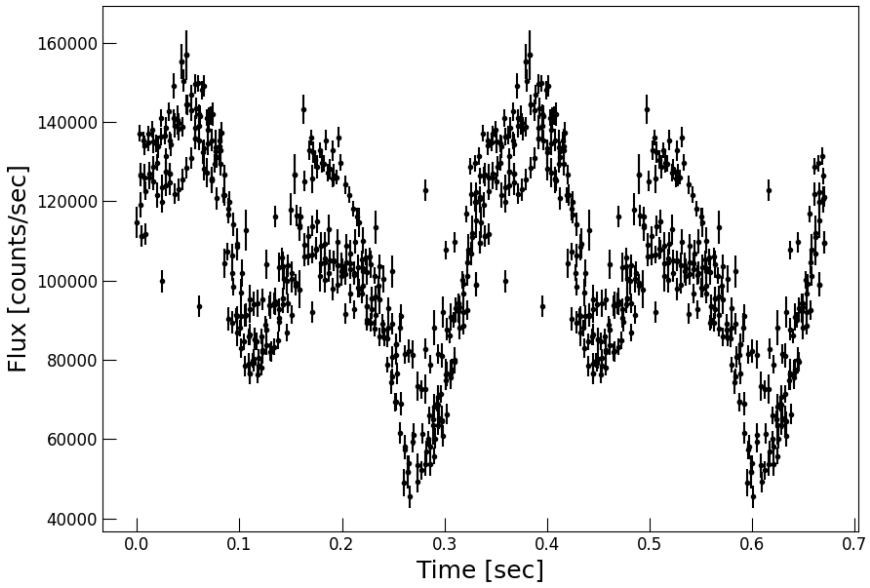

Fig. 8. Folded light curve for two cycles of the brightness oscillation accurately restored in the epoch folding analysis. The vertical axis is offset by the average flux of the raw data.

3.3 TIME VARIATION OF THE LIGHT CURVE

In section 3.2, we determined the angular velocity with fairly good accuracy from the light curve obtained in the second observation, while Fig. 8 shows that the data points scatter relatively largely compared to the error bars. In particular, we can find that the scatter is large at the horizontal axis value of about 0.2 s. Although the epoch folding analysis assumes that the brightness oscillation is coherent, the period and profile might be slightly variable in the actual observations, possibly causing the scatter in the folded light curve. To verify the possibility of the time variation of the light curve, the light curve is divided into three sections of 133 data points each, color-coded red, green, and blue in the sub figure of Fig. 9, and epoch folding analysis is performed for each section. As summarized in Table 2, the oscillation frequencies of the data in the red, green, and blue sections result in 1074.7, 1075.2, 1074.2 deg/s, respectively, indicating that the period is almost constant. Therefore, it is found that the angular velocity hardly decreases due to air resistance on a time scale of about 60 s. Fig. 9 shows the folded light curves for two cycles of the brightness oscillation. The colors of the folded light curves in Fig. 9 correspond to those of the light curve in the sub figure in Fig. 9. The profiles in Fig. 9 differ significantly among the three sections. In particular, the profile of the section colored by blue is sharper than those of the sections colored by the other colors, and also shows a phase shift. The time variation of the profiles is likely to imply the slight change of the attitude of the 3U CubeSat in the second observation.

Table 2. Summary of the estimated oscillation frequencies.

Optically observed data	
Whole data	1074.6±1.0 deg/s
Section 1 (Red)	1074.7±3.6 deg/s
Section 2 (Green)	1075.2±1.6 deg/s
Section 3 (Blue)	1074.2±1.7 deg/s
Telemetry data	1074 deg/s

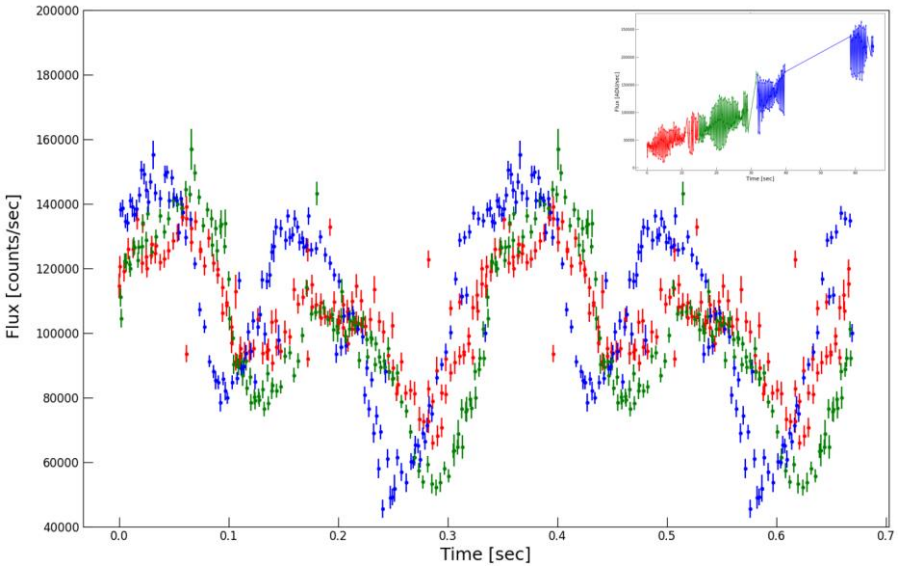

Fig. 9. Folded light curves of the three sections for two cycles of the brightness oscillation. The colors of the folded light curves correspond to those of the light curve in the sub figure. The vertical axis is offset by the average flux of the raw data.

3.4 COMPARISON WITH SUNLIGHT ILLUMINATION MODEL

We compare the folded light curve obtained in the second observation with a sunlight illumination model to obtain additional information other than the angular velocity. The illumination model is summarized as an infographic in Fig. 10, where a simple 10 cm x 10 cm x 34 cm cuboid is adopted as the illumination target, ignoring the detailed structure of the 3U CubeSat. Since each surface of the spinning cuboid reflects the incident sunlight in the direction of the observer, we need to consider the angular dependence of the reflectance of each surface. The angular dependences of the specular and diffuse reflection components are assumed to be a gauss function with a width of 10 degrees centered at the direction of the specular reflection and the Lambert's cosine law, respectively. Because the solar phase angle can be calculated to be 40-150 deg based on the TLE data of the second observation, the average angle of 90 deg is applied for the solar phase angle in the illumination model, as shown in the top right panel of Fig.10. In addition, only one axis is considered as the rotation axis for simplicity. In this case, the rotation axis is unlikely to be perpendicular to the plane containing the sun, satellite, and observer, because narrow peaks due to the specular reflection, as shown in Fig. 5, are expected to be observed every cycle. Hence, we assume that the rotation axis lies in the plane containing the sun, satellite, and observer. The light curve is simulated by calculating the total intensity of the observed reflection light with the cuboid spinning, and fits to the observed data to estimate the parameters, such as the rotation axis and the reflectance of each surface.

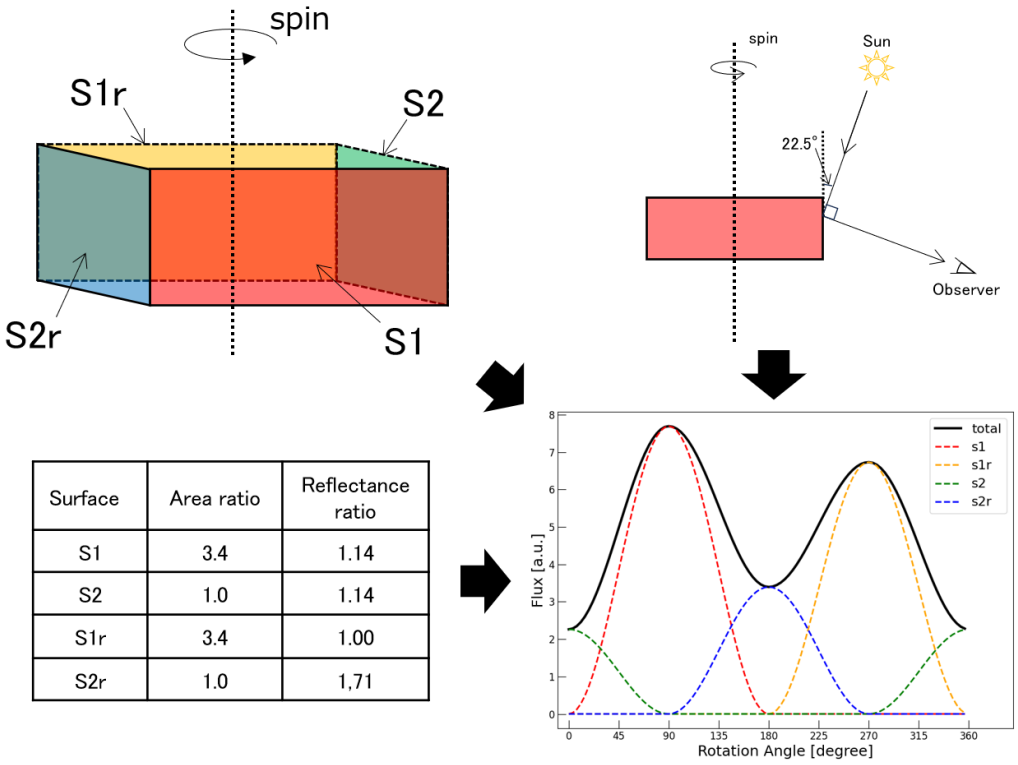

Surface	Area ratio	Reflectance ratio
S1	3.4	1.14
S2	1.0	1.14
S1r	3.4	1.00
S2r	1.0	1,71

Fig. 10. Infographic of the simple sunlight illumination model compared with the folded light curve in Section 3.4.

Fig. 11 shows the fitting result using the illumination model described above, indicating that the illumination model does well at reproducing the overall profile of one period. The 3U CubeSat is less likely to rotate around the long axis of the cuboid, because the reflectance of the adjacent 34 cm x 10 cm surfaces must be significantly different to reproduce the large peak-to-valley ratio of the two broad peaks in one period of the folded light curve. Thus, the rotation around the short axis is reasonable compared to that around the long axis on the basis of the profile of the folded light curve, since the areas are more than three times different between 34 cm x 10 cm and the 10 cm x 10 cm surfaces and the surface materials are also likely to be different. Therefore, as shown in the bottom right panel of Fig. 10, the reflection lights of the 34 cm x 10 cm and 10 cm x 10 cm surfaces dominate the light curve at the two peaks and two valleys, respectively. Furthermore, the difference in the peak intensities between the two broad peaks can be reproduced by applying for different reflectance of the front and back surfaces of 34 cm x 10 cm, suggesting the difference in the structure of each surface of the 3U CubeSat.

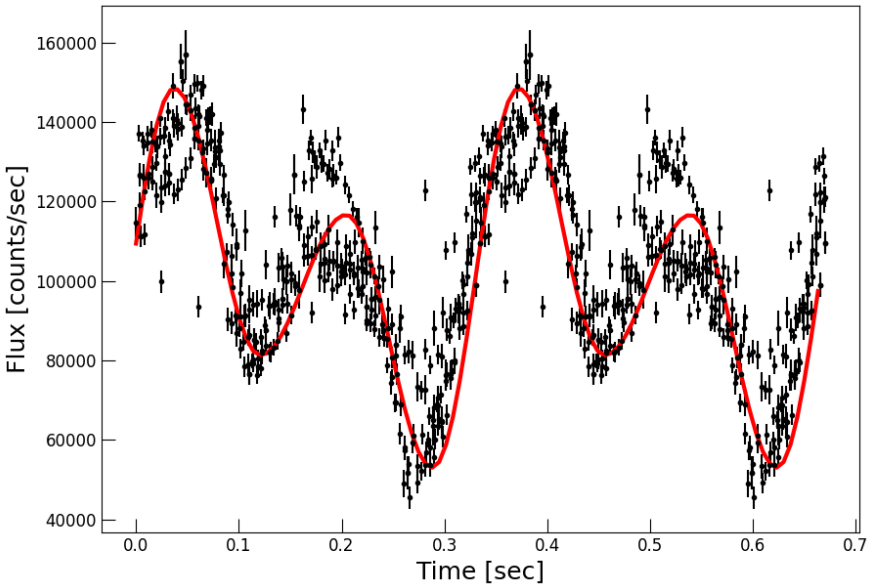

Fig. 11. Fitting result of the folded light curve for two cycles in Fig. 8 using a simple illumination model.

4. CONCLUSION

We perform tracking observations of the 3U CubeSat with optical telescope equipped in OSMC, and successfully detected the signals throughout the observations. In particular, the light curve obtained in the second observation shows a brightness oscillation, which is expected to originate from the rotation motion of the CubeSat. By conducting the Fourier and the epoch folding analyses on the brightness oscillation, the angular velocity of the satellite can be estimated with a high precision. The angular velocity of 1074.6±1.0 deg/s thus estimated is consistent to that estimated from the telemetry data, which strongly supports that the brightness oscillation of the light curve is due to the satellite rotation. In addition, we also find that the profiles of the one-period light curve, which is obtained by dividing the light curve into three sections and performing the epoch folding analysis on each section, show time variability. The time variation of the profiles could imply the slight change of the attitude of the 3U CubeSat in the second observation. Finally, the one-period light curve is compared with the illumination model. The best fitted model parameters suggest that the 3U CubeSat does not rotate around its long axis but its short axis and the structure of each surface of the 3U CubeSat is slightly different. Hence, we can confirm that the optical observation of the CubeSats is effective in detecting and characterizing them, which can contribute to ensuring safety in orbit as well as to the sustainable and secure use of outer space.

5. REFERENCES

[1] T. Endo, T. Tsuchikawa, T. Anada, H. Ono, and H. Tsuji. Simulating the Photometric Light Curve of Artificial Satellites in GEO used with a Ray-Tracing, In Advanced Maui Optical and Space Surveillance Technologies Conference, id.94, 2023.

[2] T. Endo, H. Ono, J. Suzuki, T. Ando, and T. Takanezawa. Satellite Type Estimation from Ground-based Photometric Observation. In Advanced Maui Optical and Space Surveillance Technologies Conference, 922–930, 2016.

[3] T. Fujiwara, K. Nishiyama, S. Okumura, and T. Nimura. Simultaneous photometry and spectroscopy of GEO satellites. Proceedings of the 9th Space Debris Workshop, (B10):215-239, 2021.
[4] F. R. Hoots, and R. L. Roehrich, Models for propagation of the NORAD element sets. Spacetrack Report #3, U.S. Air Force Aerospace Defense Command, Colorado Springs, 1980.
[5] D. A. Vallado, P. Crawford, R. Hujsak, and T. S. Kelso, Revisiting spacetrack report #3. In Proceedings 2006 AIAA/AAS Astrodynamics Specialist Conference and Exhibit, Vol. 3, 1984–2071, 2006.
[6] S. Okumura, K. Nishiyama, A. Asami, S. Urakawa, T. Sakamoto, N. Hashimoto, and N. Takahashi. Status of the optical observations of space debris at the Bisei Spaceguard Center. Proceedings of the 6th Space Debris Workshop, (G1):403–415, 2014.
[7] S. Okumura. Optical Observations of Space Debris at the Bisei Spaceguard Center. Proceedings of the 7th Space Debris Workshop, (G3):437–456, 2016.